

# Laser infrared photothermal radiometry of electronic solids: Principles and applications to industrial semiconductor Si wafers

Andreas Mandelis<sup>a)</sup>

Photothermal and Optoelectronic Diagnostics Laboratories (PODL), Department of Mechanical and Industrial Engineering, University of Toronto and Materials and Manufacturing Ontario, Toronto M5S 3G8, Canada

Yan Riopel

Process Engineering, MITEL S.C.C., Bromont, Quebec JOE 1L0, Canada

(Received 13 August 1999; accepted 19 November 1999)

The physical principles and application case studies of the novel diagnostic technique of laser infrared photothermal radiometry (PTR) of semiconductors are presented. Following superband gap optical excitation, the signal consists of two contributions, one due to the de-exciting carrier density (plasma wave) and another from direct absorption and heating of the lattice (thermal wave). Multiparameter fits to frequency-domain amplitude and phase data have been developed to reliably measure recombination lifetime,  $\tau$  surface recombination velocities (front and back surface), electronic, and thermal diffusivities. Applications case studies are presented, which demonstrate that lifetime measurements using PTR provide a most sensitive, convenient, and nonintrusive, remote industrial semiconductor metrology. The new metrology combines the features of several laboratory and commercial techniques currently available for industrial wafer (substrate and process) characterization (e.g., thermorefectance, microwave reflectance, and surface photovoltage). The technology is capable of being used as a sensitive control of ion implantation, contamination monitor during oxidation and wafer cleans, and photoexcited carrier recombination lifetime measurements. © 2000 American Vacuum Society. [S0734-2101(00)07502-3]

## I. INTRODUCTION

This article introduces principles and applications of a novel diffusion-wave technique based on an optoelectronic infrared photothermal radiometric (PTR) signal source, which usually dominates industrial quality electronic materials, particularly Si wafers.<sup>1</sup> Following superband gap optical excitation, the harmonically generated PTR signal consists of two contributions: one from the de-exciting and diffusing modulated carrier density (a diffusion wave called the ‘‘plasma wave’’), and another from direct absorption and nonradiative energy conversion (heating) of the lattice (‘‘thermal wave’’). The plasma-wave component is generated by direct infrared (IR) emission from photoexcited carriers (electrons or holes), each free carrier acting as an individual Planck radiator. Therefore, the signal carries information about the density of photogenerated free carriers and their subsequent recombination kinetics, a measure of the electronic trap densities and of the electronic quality of the semiconductor material.

## II. PTR OF SEMICONDUCTORS

The measurements of photoexcited excess carrier lifetime and activation energies in a semiconductor are useful in the characterization of the electronic quality of semiconductor materials and in evaluating the performance of working semiconductor devices. The noncontact method of frequency-domain PTR detection has been shown to be promising for remote on-line or off-line impurity/electronic

defect diagnostics.<sup>2</sup> According to a statement of Kirchhoff’s Law of Detailed Balance reflecting conservation of energy, *at thermodynamic equilibrium the rate of emission of blackbody radiation from the surface and throughout the bulk of a material can be measured from, and is exactly equal to, the rate of absorption of the radiation incident on the material per wavelength interval.* Therefore, the IR emission spectrum for a de-excitation process in a semiconductor can be obtained directly from its (usually better known) absorption spectrum. In PTR detection, it is rather the reverse application of Kirchhoff’s Law that is exploited: Optical absorption of a laser beam in the ultraviolet, visible, or near-IR (superband gap) spectral range in Si, for example, results in electronic excitation, followed by complex ultrafast intraband decay processes, and ultimately by much slower interband recombination kinetics. A fraction of the de-exciting electronic cloud recombines upon emission of IR (blackbody) radiation, *which is equivalent to surface and bulk absorption of the same IR flux integrated over the same depth coordinate*, in agreement with Kirchhoff’s Law. The excess energy due to carrier thermalization and any direct lattice absorption and optical-to-thermal energy conversion, are also detected as an additional increase in blackbody emission at low modulation frequencies (<1 kHz).<sup>3</sup> Therefore, signal analysis can be done entirely within the framework of free carrier diffusion and recombination under harmonic excitation conditions (a plasma wave)<sup>1</sup> at higher frequencies.

A schematic diagram of the experimental apparatus is shown in Fig. 1. An Ar-ion laser (514 nm) modulated by an acousto-optic modulator is directed onto the sample surface. The beam is broadened with a diffuser to attain a larger

<sup>a)</sup>Electronic mail: mandelis@mie.utoronto.ca

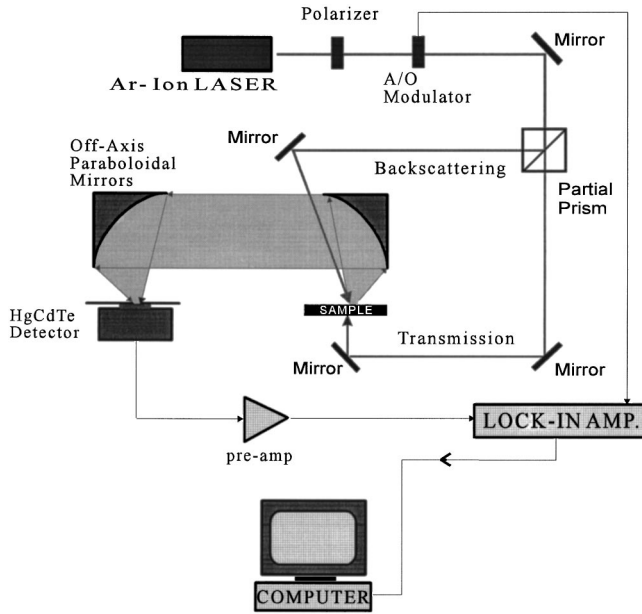


Fig. 1. Schematic diagram of typical laser photothermal infrared radiometric setup for semiconductor diagnostics and metrology.

spotsizes for one-dimensional analysis. A lens can be placed after the diffuser to achieve a sharp focus with spotsizes of approximately  $25 \mu\text{m}$ . The emitted IR radiation from the sample surface is collected and focused onto the detector using two off-axis paraboloidal mirrors. The detector is a liquid  $\text{N}_2$  cooled HgCdTe element with an active area of  $1 \text{mm}^2$  and a spectrally selective range of  $2\text{--}12 \mu\text{m}$ . A germanium window with a transmission bandwidth of  $2\text{--}14 \mu\text{m}$  is mounted in front of the detector to block any visible radiation from the pump laser. The detector signal is preamplified before being sent into the lock-in amplifier. The two lock-in amplifier outputs, amplitude, and phase, are recorded across a range of laser modulation frequencies.

### A. PTR of $\text{SiO}_2/\text{Si}$ metal-oxide-semiconductor MOS capacitors

The theoretical analysis of the dominant electronic component of the PTR signal from a semiconductor of thickness  $L$ , under high-absorption conditions ( $514 \text{nm}$ ) gives<sup>4</sup>

$$\Delta Q = \frac{N_0}{\sigma_n^2 D_n + \sigma_n s_1} C(\lambda_1, \lambda_2) \left[ \frac{(1 - e^{-\sigma_n L})^2}{1 + \Gamma_1 e^{-2\sigma_n L}} \right], \quad (1)$$

where  $N_0$  is the number of photoinjected  $n$ -type carriers at the surface,  $s_1$  is the front surface recombination velocity and the complex plasma-wave vector  $\sigma_n$  is defined as

$$\sigma_n = \sqrt{\frac{1 + i\omega\tau}{D_n \tau}}, \quad (2)$$

where  $D_n$  is the ambipolar carrier diffusion coefficient and  $\tau$  is the recombination lifetime.  $C$  is an instrumental constant.  $\lambda_1$  ( $\lambda_2$ ) is the lower (upper) limit of the detection bandwidth of the infrared detector. Also,  $\Gamma_1 = (D_n \sigma_n - s_1) / (D_n \sigma_n + s_1)$ .

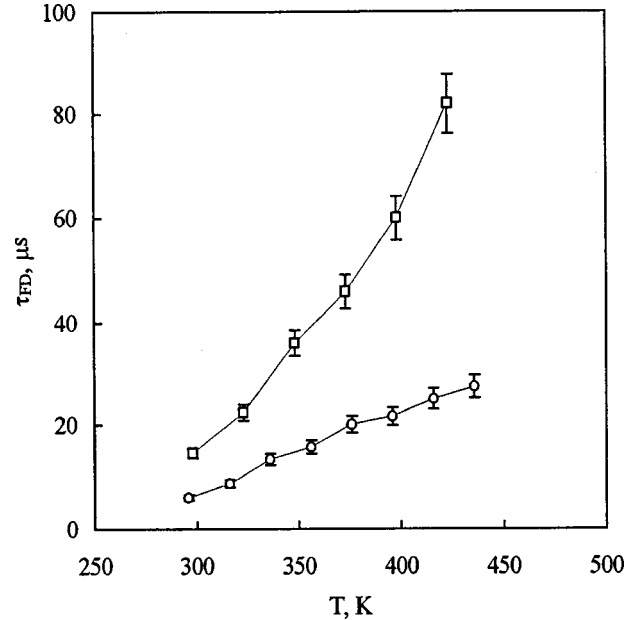


Fig. 2. PTR lifetime temperature dependencies of sample W1 ( $\circ$ ) and W2 ( $\square$ ).

Off-line quality control analysis of  $\text{SiO}_2/\text{Si}$  interfaces of full-size 4 in. Si wafers with MOS capacitor structures has been performed using PTR. A fitting procedure which uses the amplitude and phase frequency responses has been developed and has been shown to be quite sensitive to changes in carrier diffusivity ( $D_n$ ), carrier lifetime ( $\tau$ ), and surface recombination velocity ( $s$ ).<sup>4</sup> Figure 2 shows the PTR lifetime temperature dependence of two samples W1 (Al-gated MOS structure) and W2 (polysilicon-gated MOS structure), obtained by fitting the data to Eq. (1). The increase in  $\tau$  with temperature observed for both wafers follows the Shockley–Reed–Hall theory,<sup>5</sup> which assumes that the thermally increased density of intrinsic carriers fills up existing trapping sites and thus increases the photoinjected carrier lifetime. The corresponding Arrhenius plots of the PTR lifetimes and the calculated activation energies are presented in Fig. 3. The activation energy value of  $\Delta E = 0.21 \text{eV}$  obtained for sample W2 is probably due to the near-interface shallow electron traps produced during the gate layer growth. The lifetime information obtained in Fig. 2 shows that the poly-Si gate MOS devices are predicted to exhibit better performance than the metal-gated ones, as expected from the relative unavailability of metallic deep levels in the former capacitors, which are known to act as lifetime killers.

### B. Wafer contamination control by PTR $\tau$ measurements

Equation (1) shows that at low modulation frequencies and for small surface recombination velocities, the PTR signal is real and is given by

$$\Delta Q = N_0 C_2(\lambda_1, \lambda_2) \left( \frac{\tau}{D_n} \right) \left[ \frac{(1 - e^{-L/\sqrt{D_n \tau}})^2}{1 + e^{-2L/\sqrt{D_n \tau}}} \right]. \quad (3)$$

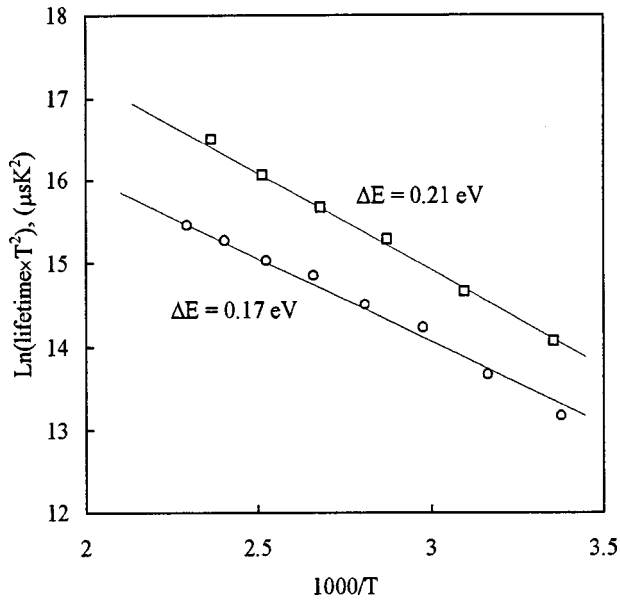


FIG. 3. Arrhenius plots of the PTR-measured lifetimes in Fig. 1.

Therefore, the amplitude becomes directly proportional to the photoinjected carrier lifetime, provided that the wafer thickness is large compared to the direct current carrier diffusion length  $\sqrt{D_n \tau}$ . This feature allows the quick characterization of process wafers. Six 4 in. diameter floating zone (FZ) *p*-type Si wafers, 10–15  $\Omega\text{cm}$ , with nominal lifetime  $> 100 \mu\text{s}$ , and thickness 540  $\mu\text{m}$ , each with a different number of gate oxidation treatments, were tested. After each oxidation cycle a specified thickness of oxide was removed, so that all wafers had the same 350  $\text{\AA}$  of oxide layer. The values of the carrier lifetimes obtained from the fits of the amplitude responses are shown in the histogram of Fig. 4. The effects of oxidation history are manifested in terms of a dramatic decrease of this parameter with the number of oxidation treatments. It is well known that oxidation is a major source of Si wafer contamination by heavy metals and other impurities and PTR is shown to be a sensitive technique for monitoring furnace contamination.

### C. Ion implantation metrology

Ion implantation is a very important technological process in the modern microelectronics industry. It is widely recognized that integrated circuit performance and yield are strongly dependent on the accuracy and uniformity of the implanted ion dose. This is especially true for some critical implantation steps such as the low-dose implant adjustment of the threshold voltages of the integrated circuit. Experimental PTR-amplitude and phase-frequency scans were obtained from the near-center region of 36 Si wafers (B-doped,  $\rho \sim 14\text{--}24 \Omega\text{cm}$ , thickness 510–520  $\mu\text{m}$ ) implanted with phosphorus to various doses from  $5 \times 10^{10}$  to  $1 \times 10^{16}$  ions/ $\text{cm}^2$  (12 different doses) at each of the three implantation energies: 50, 100, and 150 keV. The phosphorus implantation was performed through a thin oxide layer at room temperature. A nonimplanted Si wafer from the same lot was used as a reference. Figure 5 represents the results of the

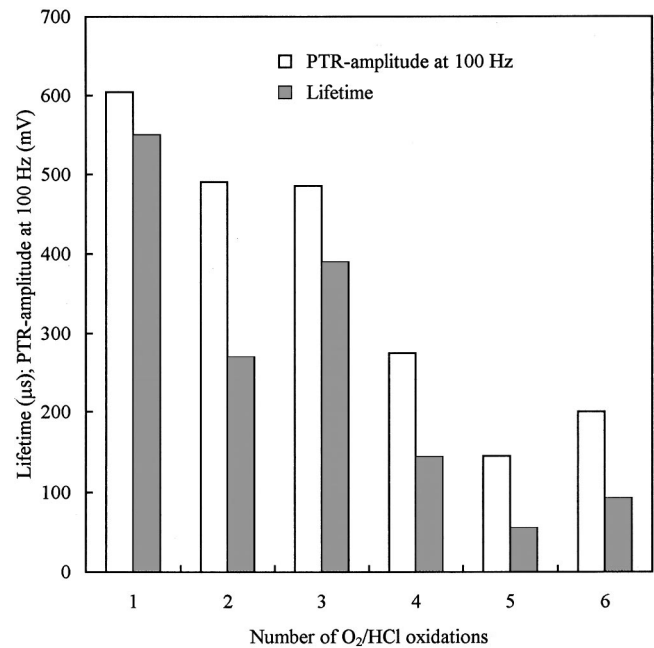


FIG. 4. Lifetime histogram for six FZ *p*-type Si wafers subjected to up to four oxidation cycles. Wafer Nos. 1–6 were rinsed and dried. Wafer Nos. 2–6 subsequently underwent one or more oxidations and HF etches. No 1:  $\text{O}_2/\text{HCl}$  oxidation (OX) only; No. 2: 1 HF+2 OX; No. 3: 2 HF+3 OX; No. 4: 3 HF+4 OX; No. 5: 4 HF+5 OX; and No. 6: 5 HF+6 OX.

PTR-amplitude and phase-frequency scans obtained from the nonimplanted reference wafer and from 12 wafers implanted at 50 keV. For the nonimplanted wafer the PTR signal exhibits carrier plasma wave dominated behavior with the PTR amplitude saturated at low modulation frequencies, Fig. 5(a), and the PTR phase tending to saturate at  $-90^\circ$  along the high frequency edge, Fig. 5(b). Simultaneous fitting of the experimental amplitude and phase data for the reference sample using the corresponding theoretical model yield the following values: minority carrier lifetime  $\tau = 10.5 \mu\text{s}$ , carrier diffusivity  $D_n = 30 \text{ cm}^2/\text{s}$ , surface recombination velocity  $s = 100 \text{ cm/s}$ , thermal diffusivity  $D_{\text{th}} = 0.8 \text{ cm}^2/\text{s}$ , and the relative weight of the carrier plasma and thermal components in the total PTR signal, expressed as a ratio of the plasma-to-thermal coefficients in the expression for the PTR signal<sup>1</sup>  $\eta = 1.6 \times 10^3$  a.u.

In the carrier plasma-dominated frequency region, the PTR signal has been found to be extremely sensitive to the damage introduced by ion implantation even at low doses and energies. At 10 kHz modulation frequency the difference between the PTR amplitudes from the nonimplanted wafer and the wafer implanted with the lowest dose/energy ( $5 \times 10^{10} \text{ cm}^{-2}$ , 50 keV) is more than one order of magnitude, Fig. 5(a), thus allowing for the monitoring of ion implantation with doses and/or energy much lower than these values. The same quantitative analysis of the PTR-amplitude and phase-frequency responses obtained for 100 and 150 keV implanted sets of Si wafers further allowed the monitoring of the variations of the carrier lifetime with implantation dose and energy and no annealing, Fig. 6. As the implantation dose/energy increases,  $\tau$  remains unchanged and equal to

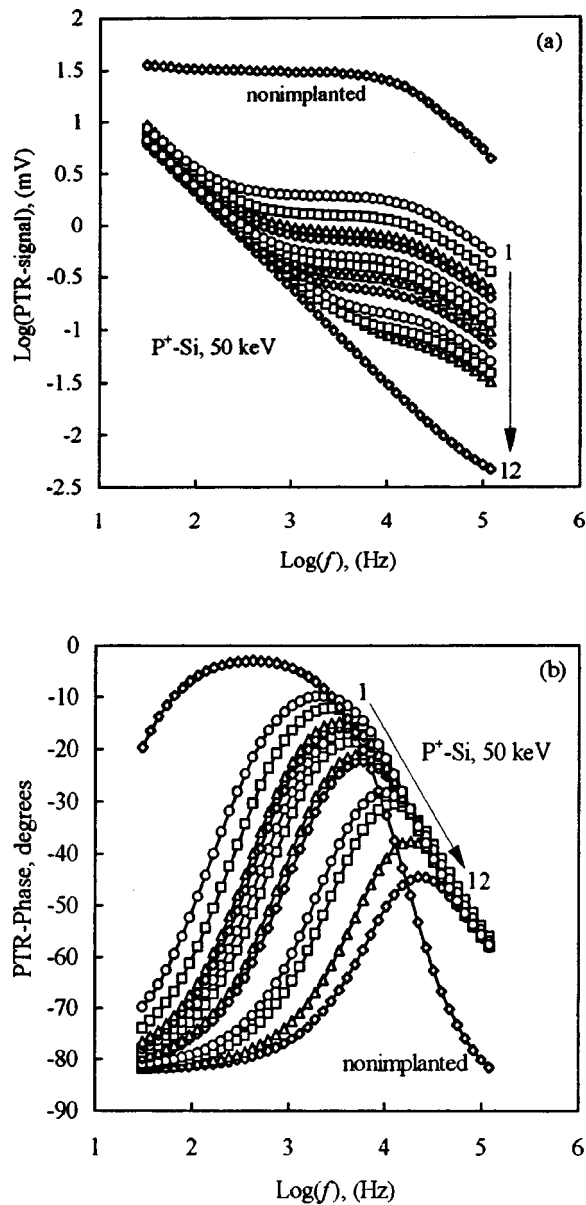


FIG. 5. Experimental PTR amplitude (a) and phase (b) frequency responses obtained from the nonimplanted reference wafer and Si wafers implanted with P<sup>+</sup> ions of 50 keV energy to various doses (ions/cm<sup>2</sup>): (1)  $5 \times 10^{10}$ ; (2)  $1 \times 10^{11}$ ; (3)  $5 \times 10^{11}$ ; (4)  $1 \times 10^{12}$ ; (5)  $5 \times 10^{12}$ ; (6)  $1 \times 10^{13}$ ; (7)  $5 \times 10^{13}$ ; (8)  $1 \times 10^{14}$ ; (9)  $5 \times 10^{14}$ ; (10)  $1 \times 10^{15}$ ; (11)  $5 \times 10^{15}$ ; (12)  $1 \times 10^{16}$ .

that in a reference wafer ( $\sim 10 \mu\text{s}$ ) up to a threshold value of the dose ( $\sim 10^{12} \text{ cm}^{-2}$ ) and then starts to decrease with a rate which is implantation-energy dependent, Fig. 6. This effect is related to the fact that the PTR technique is measuring the photoexcited carrier lifetimes in layers deeper than the thickness of the implanted layer ( $< 1 \mu\text{m}$ ). The extent of the probed (and averaged) layer is determined by the harmonic diffusion length of the carriers:  $L(\omega) = \sqrt{D_n \tau / (1 + i\omega\tau)}$ . Thus, the value of  $\tau$  in implanted Si wafers is unaffected by damage introduced by ion implantation to the uppermost layer until the effective depth of the electronically sensitive defects significantly exceeds the thickness of the implanted layer at high doses and/or energies.

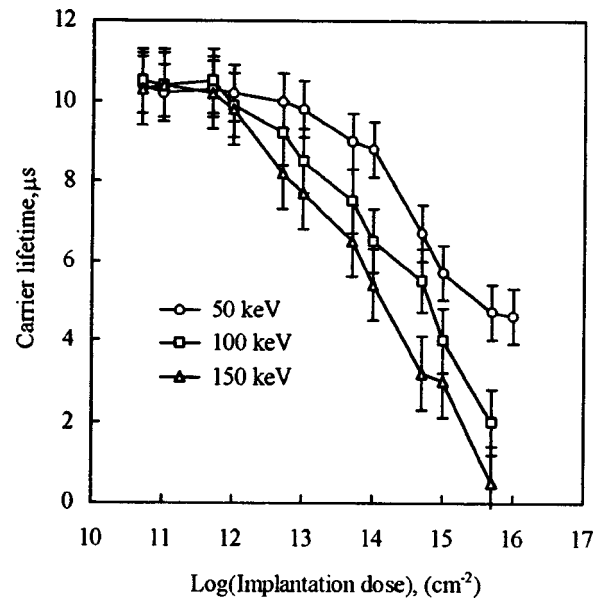


FIG. 6. Values of the minority carrier lifetime evaluated from PTR amplitude and phase frequency responses as a function of implantation dose for implantation energies of 50, 100, and 150 keV.

### III. CONCLUSIONS

In this article the physical and mathematical foundations of laser infrared PTR as a novel technology for Si wafer electronic quality characterization have been described. The presented (and other) case studies have demonstrated that lifetime measurements using PTR provide a most sensitive, convenient, and nonintrusive, remote industrial semiconductor metrology, which combines the features of several laboratory and commercial techniques currently available for industrial wafer (substrate and process) characterization (e.g., thermoreflectance, microwave reflectance, and surface photovoltage). The technology is capable of being used as a sensitive control of ion implantation, contamination monitoring during oxidation and wafer cleans, and photoexcited carrier recombination lifetime measurements. In the near future PTR is expected to advance toward parallel signal processing and nearly-real-time wafer-surface lifetime mapping by use of fast ( $> 1 \text{ kHz}$ ) charge coupled device imagers.

### ACKNOWLEDGMENTS

The support of Materials and Manufacturing Ontario (MMO) and the Natural Sciences and Engineering Research Council of Canada (NSERC) is gratefully acknowledged.

<sup>1</sup>P. Salnick, A. Mandelis, H. Ruda, and C. Jean, *J. Appl. Phys.* **82**, 1853 (1997).

<sup>2</sup>A. Mandelis, *Solid-State Electron.* **42**, 1 (1998).

<sup>3</sup>G. Busse and H. G. Walther, in *Photothermal and Photoacoustic Science and Technology*, edited by A. Mandelis (Elsevier, New York, 1992), Vol. 1, p. 205.

<sup>4</sup>P. Salnick, C. Jean, and A. Mandelis, *Solid-State Electron.* **41**, 591 (1997).

<sup>5</sup>W. Shockley and W. T. Read, *Phys. Rev.* **87**, 835 (1952); R. N. Hall, *ibid.* **87**, 387 (1952).